EVALUATING SNOWMELT MODELING METHODS OF DIFFERENT COMPLEXITIES AT A WATERSHED IN THE CANADIAN PRAIRIES

Purushottam Raj Singh[1], Thian Yew Gan[2] and Adam Kenea Gobena[2]

ABSTRACT

Three snowmelt models of different degrees of model complexity and data requirement were used to simulate snow accumulation and ablation processes for a watershed in the Canadian Prairies. Results show that modifying the popular temperature index method by incorporating near-surface soil temperature as an additional predictor to air temperature could considerably improve the model performance. In addition, the modified method could achieve hourly simulation results that are comparable to a physically based energy balance method. Majority of the improvement in the modified temperature index method occurs when the melt rate is varied as a function of near-surface soil temperature. (Keywords: snowmelt, modeling, MacKenzie River, energy balance)

INTRODUCTION

Basin-scale snowmelt runoff models that simulate the snow accumulation and melt processes can essentially be grouped into two basic classes, namely the temperature index or degree-day method (e.g., Riley et al., 1972; Martinec and Rango, 1986; Kane et al., 1997) and the energy balance method (e.g. Anderson, 1968; Kondo and Yamazaki, 1990; Jordan, 1991; Tarboton and Luce, 1996; Jin et al., 1999). While the temperature-index models relate the melt rate to a meteorological variable (often air temperature) through a melt factor, energy balance models are based on the detailed physics of snow accumulation and ablation processes with massive, good quality data requirements. Energy balance models are generally not suitable for operational implementation due to lack of the necessary data.

Apart from process details, basin snowmelt is also affected by the spatial variability of basin terrain characteristics, which can be accounted for using distributed or semi-distributed modeling (Bathurst and Cooley, 1996). Unfortunately, the model complexity and data requirement usually increase substantially as we move progressively from lumped to fully distributed approaches. Moreover, using grid elements of fine resolution to represent heterogeneous terrain features involves many unresolved uncertainties (Kirnbauer et al., 1994), and modeling hydrological processes using rectangular grids can be artificial. Beven (1996) suggested using large scale than small-scale parameterization strategy. Blöschl (1999) argued that optimum model resolution may not exist and suggested that model resolution may be dictated by "practical considerations such as data availability and the required resolution of the predictions". Essentially, one must find a trade-off between the attainable resolution of hydrologic information retrievable from satellite data and the accuracy required.

By comparing the performance of a hierarchy of snowmelt models with varying degree of model complexity and structure, and data demand, our objective is to find a trade-off between the level of physics and data requirement for snowmelt modeling. To meet the objective, we develop three semi-distributed models based on (1) an empirical, standard temperature-index method (SDSM-TI), (2) a modified temperature-index method (SDSM-MTI), and (3) a physics-based, energy balance snowmelt model (SDSM-EBM).

DESCRIPTION OF MODELS

Standard and modified temperature index models (SDSM-TI and SDSM-MTI)

The standard temperature index model (SDSM-TI) relates snowmelt rate, m (mm d^{-1}) to air temperature (T_a) through a melt factor, M_f (mm d^{-1} °C^{-1}) as

$$m = M_f (T_a - T_{thm}) \quad (1)$$

where T_{thm} is a melt-threshold temperature. $(T_a - T_{thm})$ is an empirical index of the total amount of insolation received on a regional basis. M_f depends on the slope, aspect of the land surface (Frank and Lee, 1966), vegetation

Paper presented Western Snow Conference 2009

[1] P. R. Singh, Golder Associates Ltd., Abbotsford, BC, Canada, V2T 4S8, prsingh@golder.com
[2] T. Y. Gan, 3-133 NERF, University of Alberta, Edmonton, AB, Canada T6G 2W2, tgan@ualberta.ca
[2] A. K. Gobena, 3-019 NREF, University of Alberta, Edmonton, AB, Canada T6G 2W2, agobena@ualberta.ca

cover, and climate. Equation (1) works well only when there is a strong correlation between T_a and the dominant energy responsible for snowmelt.

In this study, a modified temperature index model (SDSM-MTI) that includes the near-surface soil temperature (T_g) as an additional predictor is proposed,

$$m = M_f(M_{rf})(T_r - T_{thm}) \quad (2)$$

where M_{rf} is an adjustment factor for M_f so as to better capture the onset of initial snowmelt and is estimated from

$$M_{rf} = \left[\beta_1 + \beta_2\left(\tan^{-1} T_g + \beta_3\right)\right]^{\psi} \quad (3)$$

where β_1, β_2, β_3 and ψ are model parameters derived through calibration (see Singh et al., 2005). As a tangent function, M_{rf} is relatively small when $T_g < 0$°C, and reaches an upper limit of one when $T_g \geq 0$°C. The effect of M_{rf} is ''felt'' mostly during the onset of snowmelt because its value approaches 1.0 when T_g approaches 0°C. The desired rate of change of M_{rf} can be achieved by adjusting the parameter ψ. T_r is a reference temperature computed as a weighted average of T_g and T_a,

$$T_r = \chi T_a + (1-\chi)T_g \quad (4)$$

where χ is also a model parameter. The rationale for the proposed modification comes from past studies that pointed out the importance of T_g as an indicator of spring snowmelt (Woo and Valverde, 1982), as well as our own empirical analysis of data observed at the Paddle River Basin (PRB) in central Alberta. Analysis of hourly data observed for 6 years during the spring season (1 March to 30 April) at PRB shows that there is a significant correlation between net radiation (R_n) and T_g at daily time step (Singh et al., 2005). Moreover, the data revealed that Pearson's correlation coefficient between T_g and R_n (ranging from 0.62 to 0.89) was mostly higher than that between T_a and R_n (ranging from 0.47 to 0.87). Since R_n generally dominates the energy balance during spring snowmelt in the Canadian Prairies (Shook, 1995), adding T_g should improve the performance of the Equation 1.

Energy balance model (SDSM-EBM)

Figure 1 shows the schematic diagram of some of the processes considered in SDSM-EBM. The model incorporates processes for snow interception by forest canopy, separate snowpack energy and mass balance for open and forested areas, separate water balance for liquid and ice phases, snow sublimation, compaction, refreezing etc. A brief description of the major model components is provided below but interested readers can find more details in Singh (2002) and Singh et al (2009).

The snow interception capacity at different levels of canopy is estimated as a function of leaf area index (LAI), forest types (Hardy and Hansen-Bistow, 1990), tree species and prevailing forest structure (Golding and Swanson, 1986). The snow interception model of Hedstrom and Pomeroy (1998) developed for the Canadian southern boreal forest, was implemented in SDSM-EBM.

Energy transfer at the snow surface and snow-soil interface is estimated from a one-dimensional, energy equation applied to a control volume of snow having upper and lower interfaces with air and ground, respectively. During melting, the snowpack is isothermal at 0°C ($T_{sp}^{t+1} = 0$) and the heat for snowmelt, Q_m, is

$$Q_m = -\left(Q_n + Q_h + Q_e + Q_p + Q_g + U\right) \quad (5)$$

where U is the cold content of snowpack in the previous time step ($U = \rho_w C_s W T_{sp}^t$), Q_n is the sum of net shortwave (Q_{sn}) and longwave (Q_{ln}) radiation (J m^{-2}), Q_h is convective or turbulent sensible heat flux (J m^{-2}), Q_e is latent heat flux (J m^{-2}), Q_p is advective heat of precipitation (J m^{-2}), Q_g is ground heat flux (J m^{-2}), ρ_w is density of water (kg m^{-3}), W is snow water equivalent (m), C_s is snowpack heat capacity (2093.4 J kg^{-1} °C^{-1}), and T_{sp} is snowpack temperature (°C). In computing U, the heat capacity of the entrapped air is neglected. Except for barren ground in the Arctic and during snowcover development, Q_g is generally negligible. The incident shortwave radiation, Q_s is converted to Q_{sn} as a function of the areal albedo of a partially ablated snowcover (α), which is taken as the larger of that retrieved from NOAA-AVHRR images or that computed from

$$\alpha = \alpha_{sn} A_{sn} + \alpha_g (1 - A_{sn}) \quad (6)$$

where α_{sn} is snow albedo estimated from an albedo decay function (Riley et al., 1972), α_g is albedo of the ground surface and A_{sn} is the fraction of snow-covered area, which is tracked using either a linear or a non-linear depletion curve (Singh, 2002; Singh et al., 2009). In forest-covered areas, α_{sn} is modified to account for the effect of litter fall fraction (Hardy et al., 1998).

The depth of snowmelt (negative flux) or the volume of liquid water frozen (positive flux), M, due to Q_m is

$$M = \frac{Q_m}{\rho_w \lambda_f \Theta} \tag{7}$$

where λ_f is latent heat of fusion of ice (335 kJ kg^{-1}), and Θ is the thermal quality of snow, which is the ratio of the heat necessary to completely melt a snowpack to that needed to produce the same quantity of melt from pure ice at 0°C.

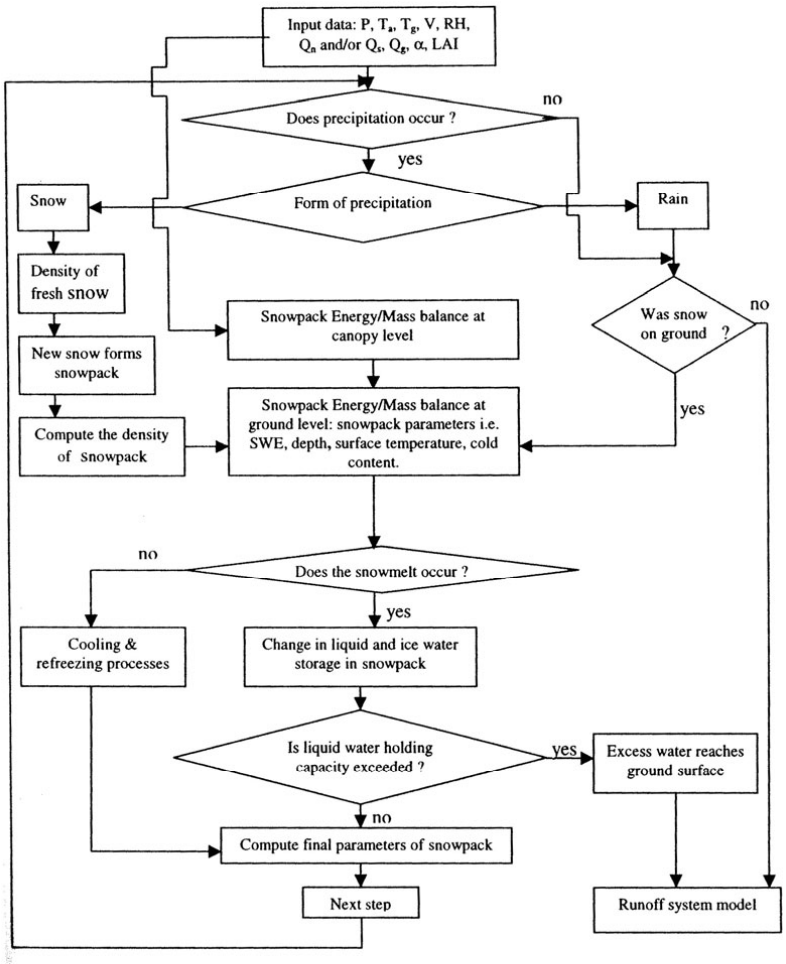

Figure 1. Schematic diagram of SDSM-EBM (Singh, 2002)

The Q_n received at the reference height is partitioned into Q_n at ground (or soil) level (Q_{ns}) and at vegetation canopy level (Q_{nc}) (Kustas et al., 1998),

$$Q_{ns} = Q_n \exp\left(\frac{-\kappa' LAI}{\sqrt{2\cos Z_s}}\right) \tag{8}$$

where $\kappa' = 0.6$ and $Q_{nc} = Q_n - Q_{ns}$.

The turbulent heat flux terms Q_e and Q_h are sensitive to atmospheric stability and require the computation of reasonably accurate surface temperature. SDSM-EBM computes the snow surface temperature using one of three simplified heat flow models, namely the force-restore method (FRM), the surface conductance method (SCM), and the Kondo and Yamazaki method (KYM). A complete description of the mathematical equations for these three models and a rigorous evaluation of the simulations can be found in Singh and Gan (2005). Here, we present results of simulations based on the SCM option only.

The snowpack water balance is evaluated separately for water and ice at both canopy and ground levels from

$$\rho_w c_s W^{t+\Delta t} T_{sp}^{t+\Delta t} = \rho_w c_s W^t T_{sp}^t + (Q_n + Q_h + Q_e + Q_g + Q_p) + Q_m \quad (9)$$

$W^{t+\Delta t}$ accounts for both the addition of precipitation (P_r or P_s) during the time step and the change in water and ice mass due to Q_e (sublimation or freezing) depending on whether T_{sp}^t is isothermal at zero or less than zero. The net energy exchange in the snowpack (Q^*) is equal to

$$Q^* = (Q_n + Q_h + Q_e + Q_g + Q_p) \quad (10)$$

If $Q^* < 0$, the snowpack is losing energy to the atmosphere (cooling), and some liquid water (if available) may be re-frozen. The amount of energy released to the snowpack (positive value) by re-freezing liquid water is given by

$$Q_m = \min(-Q^*, \rho_w \lambda_f W_{liq}^{t+\Delta t}) \quad (11)$$

The resulting change in the liquid and ice phases are given by

$$W_{liq}^{t+\Delta t} = W_{liq}^{t+\Delta t} - \frac{Q_m}{\rho_w \lambda_f} \quad (12a)$$

$$W_{ice}^{t+\Delta t} = W_{ice}^{t+\Delta t} + \frac{Q_m}{\rho_w \lambda_f} \quad (12b)$$

$$W^{t+\Delta t} = W_{liq}^{t+\Delta t} + W_{ice}^{t+\Delta t} \quad (12c)$$

The negative snowpack temperature, $T_{sp}^{t+\Delta t}$ (associated with its cold content), is then updated from Equation 9. If $Q^* > 0$, the snowpack is gaining energy from the atmosphere (heating), and in the process the negative $T_{sp}^{t+\Delta t}$ will increase until it just reaches the isothermal condition ($T_{sp}^{t+\Delta t} \rightarrow 0$). When $T_{sp}^{t+\Delta t}$ becomes positive, it is set equal to zero and Q_m is computed by Equation 9 and applied to Equations 12a and 12b to compute the new liquid and ice components of SWE.

During melt (negative Q_m) and $T_{sp}^{t+\Delta t}$ is isothermal at 0°C, water is removed as meltwater (m_{ij}) when the liquid phase increases beyond the current liquid water holding capacity (*LWHC*) of the snowpack at the expense of the ice phase, or m_{ij} is held within the pack when snowmelt first appears at the bottom of the snowpack.

$$m_{ij} = W_{liq}^{t+\Delta t} - (LWHC) W^{t+\Delta t} \quad (13)$$

where *i* is the sub-basin number and *j* is the land use type, and recommended values for *LWHC*, a function of snowpack properties and the presence of depth-hoar, are 0.02W to 0.05W (U.S. Army Corps of Engineers, 1956), and 0.05W for $\rho_{sp} < 400$ kg/m^3 (Riley et al., 1972). As meltwater contributes runoff at the bottom of snowpack, the new $W_{liq}^{t+\Delta t}$,

$$W_{liq}^{t+\Delta t} = W_{liq}^{t+\Delta t} - m_{ij} \quad (14)$$

The final SWE is computed from Equation 12c. Routing the meltwater through the snowpack is neglected because the routing time for moderately deep snow covers is usually less than the hourly time step of the model.

STUDY AREA AND DATA

The study basin is the Paddle River Basin (PRB) (53º 52' N, 115º 32' W) in Central Alberta (Figure 2). PRB has a drainage area of 265 km^2, of which about 70% is covered with coniferous and mixed forests. The basin has an average land slope of 3-5%, with elevation ranging from 749 m at basin outlet to 1000 m at the western end. PRB has a moderate hydrological response. Out of an annual mean precipitation of 508 mm (Pretula and Ko, 1982), about ¼ falls between December and April, and the basin's early April average SWE is about 70mm.

Hourly air temperature, precipitation, near surface soil temperature, wind speed, incoming solar radiation, net radiation and ground heat flux were collected using a meteorological tower set up in PRB. Details of the instruments used for data collection are provided in Biftu and Gan (2001). Data for the winter periods of 1 January to 30 April 1998, 11 November 1998 to 16 May 1999, 1 January to 30 April 2000, and 11 November 2006 to 8 May 2007 were used in this study. For brevity, these datasets will be referred to as WY 1998, WY 1999, and WY 2000, and WY 2007, respectively in subsequent sections. Three land cover classes (coniferous forest CF, deciduous (mixed) forest DF, and open area OA) were identified from a Landsat-TM image of 7 August 1996.

Snow course data (snow depth and density) were collected for each land cover using a MSC tube sampler. Additional snow data were obtained from Paddle River Headwaters snow pillow site that is operated by Alberta Environment. Hourly streamflow data for WY 1998, WY 1999, WY 2000 and WY 2007 were obtained from the Water Survey of Canada (WSC) gauging station 07BB011 (53°51'29" N, 115° 21'45" W) located on the Paddle River. The locations of the snow pillow site, gauging station and meteorological tower are shown in Figure 2. Normalized difference vegetation index (NDVI), leaf area index (LAI), surface albedo, and surface temperature were retrieved from the NOAA Advanced Very High Resolution Radiometer (AVHRR) and Landsat-TM images.

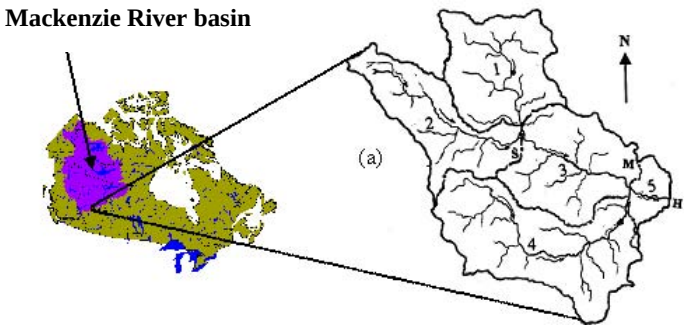

Figure 2. Map showing the location map of the Paddle River basin (PRB), the streamflow gauging station (H), the meteorological tower (M), the snow pillow site (S) and the five subbasins.

MODEL IMPLEMENTATION

To find a trade-off between modeling resolution, complexity and data availability, we developed SDSM-TI, SDSM-MTI and SDSM-EBM in a semi-distributed approach. For the test site of 265 km^2, PRB is divided into 5 sub-basins (Figure 2). At sub-basin scale, the snowmelt (M_i) for sub-basin i and at each time step is the sum of melt from each land cover, weighted by its corresponding areal fraction ϕ_j as

$$M_i = \sum_{j=1}^{n} \phi_j m_{ij} \qquad (15)$$

where n is the total number of land cover classes considered. The models are integrated into the semi-distributed physically-based model DPHM-RS of Biftu and Gan (2001). DPHM-RS accounts for Hortonian, saturated overland and subsurface runoff from each sub-basin. Surface runoff is routed to the stream channel by an average kinematic response function derived for each sub-basin. Soil moisture is modeled via a three-layer homogeneous soil profile. Water movement in the unsaturated zone is assumed to be vertical and non-interacting between sub-basins while saturated subsurface flow is simulated by a modified topographic soil index. Routing of channel flow to the basin outlet is accomplished by the Muskingum-Cunge method.

CALIBRATION AND VALIDATION RESULTS

The models were calibrated with hourly data of WY 1999, and validated with data of WY 1998, WY 2000 and WY 2007. These four winters experienced a wide range of snowfall, with WY 1999 as a record wet while WY 1998 and WY 2000 as record dry winters. The start of WY 1998 and WY 2000 was set at 1 January partly because major snowfall started late in both years, and partly to ensure that winter snow accumulation process occurred with T_g at around or below the freezing temperature.

To adequately assess the model performance, the snow models were evaluated in a multicriteria framework in terms of snow depth, SWE, runoff hydrograph, and statistics such as the coefficient of determination (R^2), the Nash-Sutcliffe coefficient (E_f), and the root mean square error (RMSE). The energy balance component of SDSM-EBM was evaluated by comparing simulated snow surface temperature with skin temperature retrieved from NOAA-AVHRR data (Singh and Gan, 2005).

Snow water equivalent and snow depth

The quality of SWE and snow depth (SD) simulations was primarily assessed by visual comparison with observed snow course data in Figures 3-6. A limited quantitative assessment of the model performance was also done by pooling together snow data for different land cover types because of the limitations in the number of

observed snow course data available. SWE and SD simulations were conducted for each subbasin and land use class, but we focus our discussion of the results predominantly on Subbasin 4 primarily because its mean elevation is closer to the mean elevation of the PRB. A summary of the statistics for Subbasin 4 is presented in Table 1. The statistics in Table 1 were computed from 12 to 14 data points and should be used with caution.

Table 1. Model performance statistics for SWE and SD simulations pooled together by land cover types for each year in the calibration and validation periods[1]

Year	Skill	SWE			SD		
		MTI	EBM	TI-R^2	MTI	EBM	TI-R^2
1998	R^2	**0.56**	0.53	0.46	**0.82**	0.74	0.61
	RMSE (%)	**36.04**	41.80	58.03	**26.61**	29.46	58.73
1999	R^2	0.62	**0.65**	0.17	**0.47**	0.41	0.47
	RMSE (%)	**7.54**	11.93	18.71	**13.43**	13.44	26.01
2000	R^2	**0.87**	0.47	0.08	**0.87**	0.34	0.48
	RMSE (%)	**18.59**	50.21	77.97	**15.88**	45.93	81.81
2007	R^2	0.00	**0.06**	0.01	0.02	**0.20**	0.13
	RMSE (%)	32.82	**35.73**	30.19	34.70	**27.26**	34.74

[1] Boldfaces indicate best value for each statistic.
[2] Melt factors were recalibrated for this model.

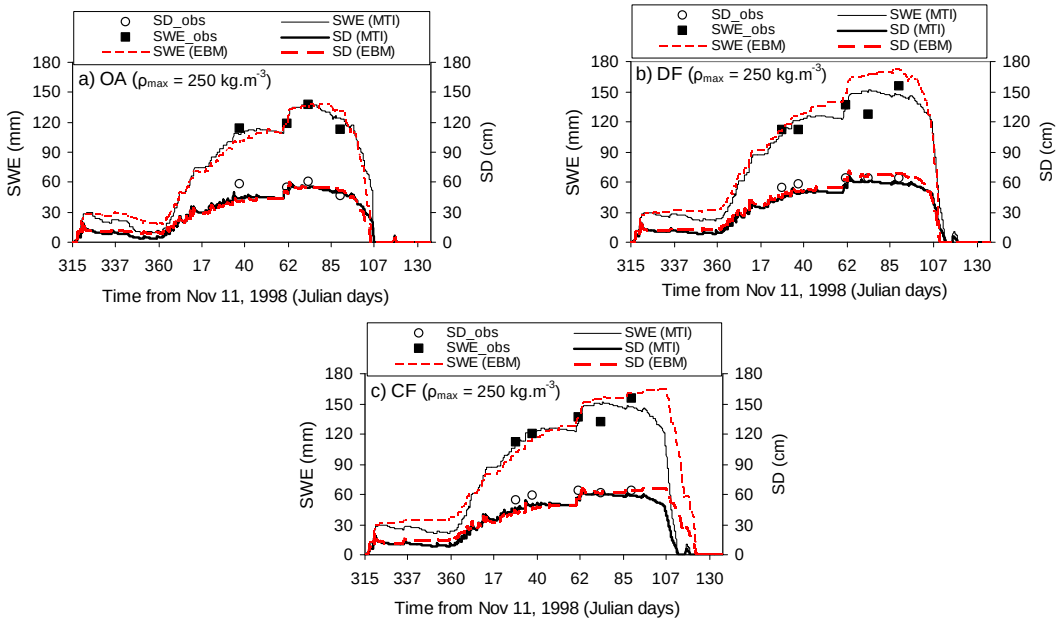

Figure 3. Comparison of observed SWE and SD to those simulated by SDSM-EBM (dashed lines) and SDSM-MTI (solid lines) during the calibration period for Subbasin 4: (a) OA, (b) DF, and (c) CF

For the calibration period of WY 1999, SWE and SD simulations from both SDSM-EBM and SDSM-MTI agree reasonably well with their observed counterparts as shown in Figure 3. For the early part of the snow accumulation, better SD simulations could be achieved using $\rho_{s,max}$ of 200 kg m^{-3} instead of 250 kg m^{-3} (figure not shown). This is in line with the anticipated increase in snow density with time. $\rho_{s,max}$ continues to change due to interaction of the snowpack with freshly fallen snow, metamorphism and settlement, and usually reaches the highest value at the end of snow accumulation period. According to Gray and Prowse (1993) dry snow densities for forest environments with shallow snow (SD < 1 m) usually reach an approximate maximum value of 250 kg m^{-3}.

SWE and SD simulations of SDSM-MTI and SDSM-EBM for the three validation periods are compared to their observed counterparts in Figure 4. Even though both models have successfully reproduced the snow accumulation and ablation dynamics in the subbasin, considerable discrepancies between the two models are observed for the DF for WY 1998 and WY 2000, as well as for both OA and DF for WY 2007. For WY 2007, preliminary daily SWE data are also available from the Alberta Environment snow pillow station shown in Figure 2. These data can offer better insight into the models' ability to capture the dynamics of snow accumulation and ablation in the basin. Since the snow pillow is located in a forested area, the simulated SWE for coniferous and deciduous forests in Sub-basin 2 were compared to the snow pillow data in Figure 5. For the coniferous forest, SDSM-EBM reproduced the snow accumulation between 1 January 2007 and 13 March 2007 perfectly. After 13 March, the model overestimated snow accumulation and similarly lagged the ablation by about 2 days. On the other hand, SDSM-MTI slightly overestimated snow accumulation up to the beginning of March and then reproduced the late season accumulation and ablation almost perfectly. For deciduous forest, SDSM-EBM overestimated snow accumulation but it accurately reproduced the dynamics of the ablation period. On the other hand, SDSM-MTI closely reproduced both the accumulation and ablation dynamics in that subbasin.

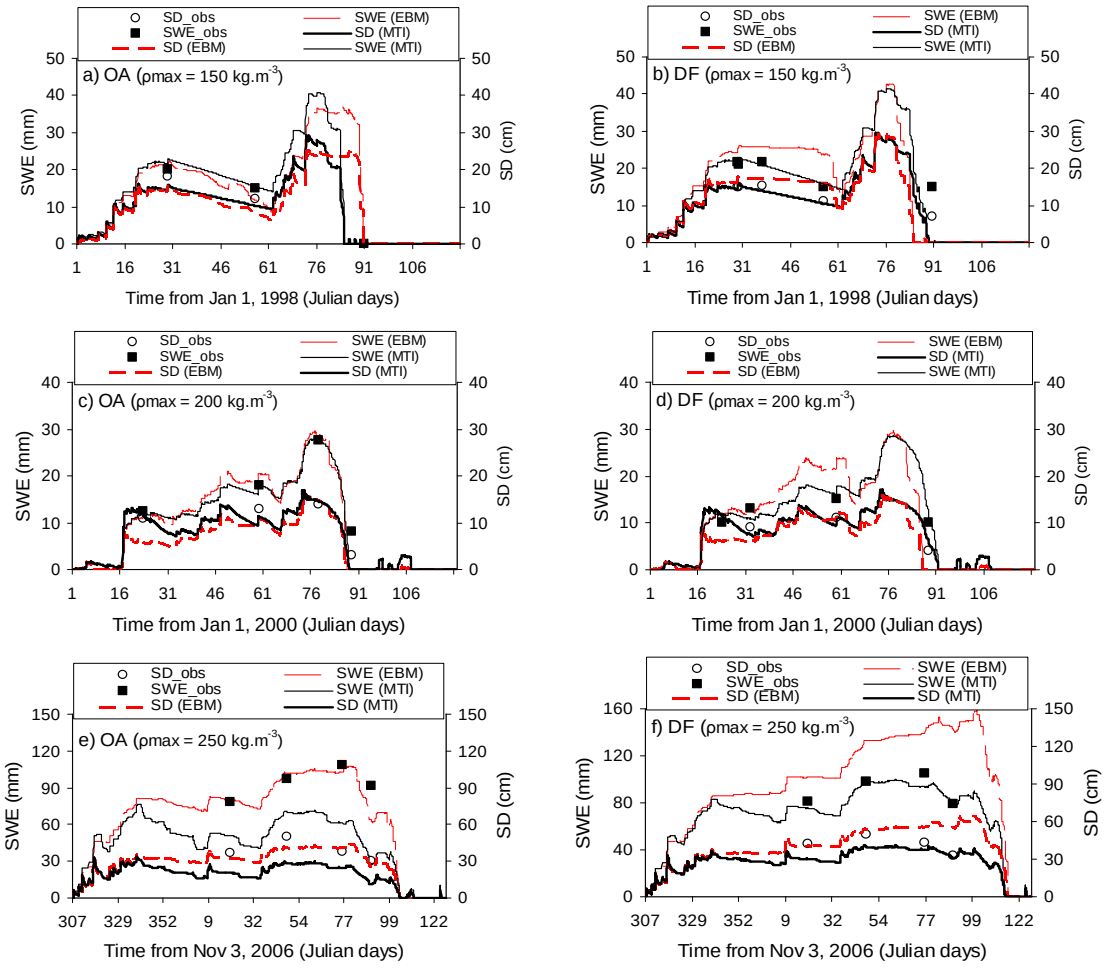

Figure 4. Comparison of observed SWE and SD to those simulated by SDSM-EBM (dashed lines) and SDSM-MTI (solid lines) during the validation stages for OA (a, c, and e) and DF (b, d, and f) of Subbasin 4

A perusal of the snow pillow data suggests that values before 1 January 2007 and after 30 April 2007 are incorrect because the observed SWE jumped from 24.4 mm on 31 December 2006 to 69.1 mm on 1 January 2007 although the precipitation gauge located at the PRB headwaters near the snow pillow recorded only 0.9 mm during those two days. Similarly, the observed SWE data indicate that the ablation process stopped on 30 April 2007 after which 28.7 mm of SWE remained on the pillow until the last day of observed data on 23 May 2007. The hourly

average air temperature recorded at our meteorological tower varied from 0.5°C to 18.8°C between 1 May and 8 May 2007. Other than lapse rate adjustment, the air temperature at the headwaters would also be expected to exhibit a similar trend, which suggests that the ablation should have continued without interruption.

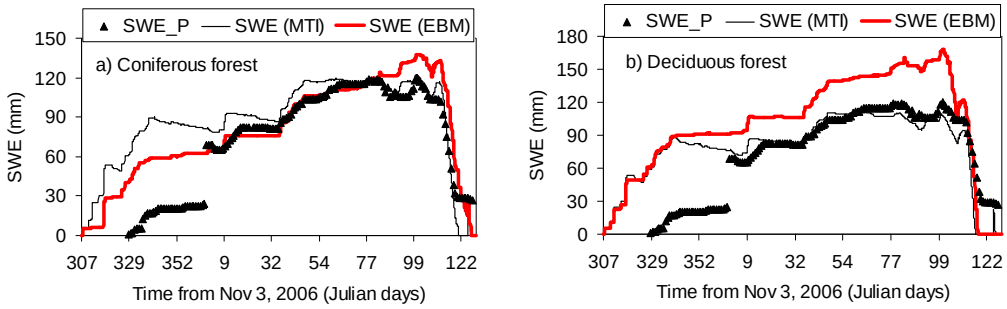

Figure 5. Comparison of daily snow pillow observations to SWE simulated by SDSM-EBM (thick line) and SDSM-MTI (thin line) for coniferous and deciduous forests of Sub-basin 2 for the 2006/07 validation year

Being an empirical model, SDSM-MTI does not properly account for the cold content of the snowpack. Even though the introduction of near-soil surface temperature partly overcomes the limitations of the standard temperature index approach, occasional warm air masses occurring in the winter may cause SDSM-MTI to over-simulate snowmelt runoff even though the heat from such warm events may not be sufficient to overcome the cold content of the snowpack. On the other hand, SDSM-EBM accounts for the cold content explicitly and should more accurately simulate snowmelt under such circumstances. This is likely the reason for the discrepancy between the two models, e.g., for the open area simulations between 7 December 2006 (Julian day 341) and 8 January 2007 (Julian day 8) (Figure 4e). During that period, SDSM-MTI simulated a reduction of about 33 mm of SWE whereas SDSM-EBM simulated a reduction of about 8 mm of SWE. For that same period, the total precipitation recorded at the gauge was only about 7 mm. For forested areas, SDSM-MTI performs relatively better by virtue of using smaller melt factors, which will partly suppress the effect occasional warm air masses occurring in winter.

To assess the improvement achieved by incorporating T_g in the temperature index model, SDSM-TI was first run with the same parameter values for SDSM-MTI with the exception of χ and ψ (Equations 2-4). When the effect of T_g was partially ignored (χ was set to 1 and ψ retained), the model performance deteriorated marginally. However, when the effect of T_g was completely ignored (i.e., ψ was set to zero and χ was set to 1, thus switching to Equation 1), the performance of the model was very poor for both calibration and validation stages for all land cover classes. These results are shown for OA and CF in Figure 6.

In order to better appreciate the improvement achieved by introducing T_g and also to perform a fair comparison between SDSM-TI and SDSM-MTI, the melt factors, M_f of SDSM-TI (Equation 1) were re-calibrated based on T_a alone. We found that we had to use artificially low M_f values for SDSM-TI to perform well at the calibration stage (Figures 6a, b), e.g., M_f of 0.03 mm hr^{-1} $^oC^{-1}$ (0.72 mm d^{-1}^{o} C^{-1}) for CF, 0.04 mm hr^{-1} $^oC^{-1}$ (0.96 mm d^{-1} $^oC^{-1}$) for DF and 0.05 mm hr^{-1} $^oC^{-1}$ (1.20 mm d^{-1} $^oC^{-1}$) for OA. However, the model performance dropped considerably when these M_f values were used for all validation stages (Figures 6c-h). Introducing diurnal and seasonal variability into the melt factor did not substantially improve the results of SDSM-TI (Singh et al, 2005). Apparently in a Prairie environment where the seasonal snow cover is shallow to moderately deep, where T_g is found to have fairly strong correlation with the net radiation (Q_n), and the onset of major snowmelt usually happens when T_g approaches 0^{o}C, using both T_g and T_a in a temperature index approach (e.g., SDSM-MTI) should generally lead to more accurate results than using T_a alone.

Streamflow simulation

The three snowmelt models were further assessed in terms of hourly simulated runoff at the outlet of the PRB within the framework of the semi-distributed hydrologic model DPHM-RS (Figure 7). At the calibration stage (Figure 7a), SDSM-EBM (R^2 = 0.85, E_f = 0.87, and *RMSE* = 1.01) and SDSM-MTI (R^2 = 0.79, E_f = 0.76, *RMSE* = 1.24) performed reasonably well. Using the percent bias (PBias) as the diagnostic measure for long term water balance (where PBias measures the difference between the average simulated and observed flow), SDSM-EBM (SDSM-MTI) shows a PBias of -10.7% (-2.8%). In terms of the timing of peak flows, both SDSM-EBM and SDSM-MTI show a tendency to lag the peak flows observed between Julian days 105 and 106 although the

accuracy of the peak flows observed on these dates is suspect since zero flows were also observed in the middle of the peak flows. The models lag the peak flow observed on Julian day 122 by about 10 hours.

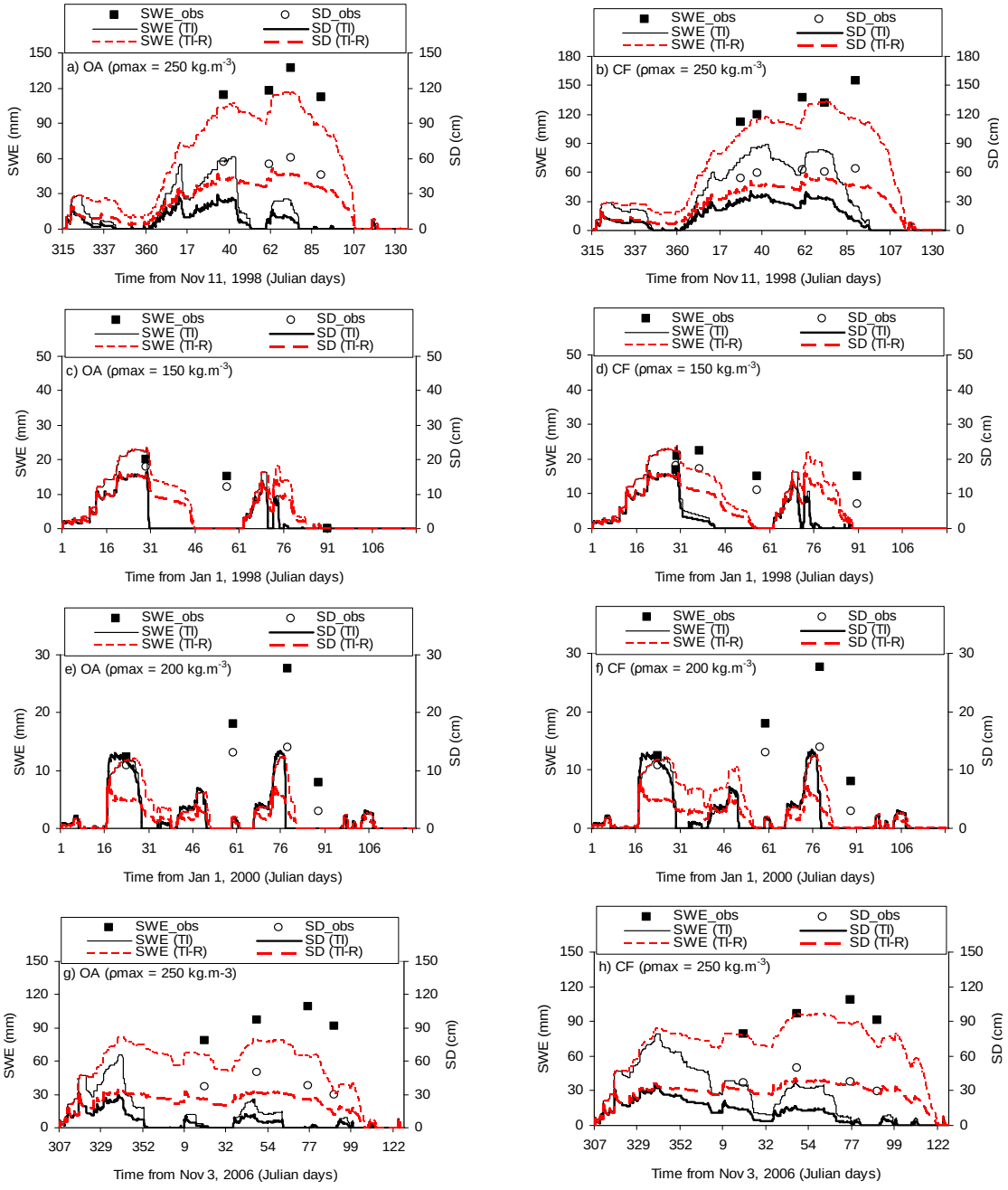

Figure 6. Comparison of observed SWE and SD to those simulated by SDSM-TI (TI, solid lines) and the SDSM-TI with recalibrated melt factors (TI-R; broken lines) during the calibration and validation stages for the OA (a, c, e and g), and CF (b, d, f and h) of Sub-basin 4

Runoff simulations for the validation periods were generally not as accurate as calibration results. This is particularly the case for the dry winters of WY 1998 and WY 2000 (Figure 7b-c). The discrepancies between simulated and observed runoff could partly be attributed to errors in the lapse rate and gradient used to distribute point temperature and precipitation measurements to sub-basins, errors in rating curve-discharge relationships due

to icing, and the "regulatory" effects of beaver dams in PRB's streamflow. The last two reasons are particularly important during dry winters such as WY 1998 and WY 2000 than during wet winters such as WY 1999. Relatively low water levels during the early part of the snowmelt season could cause the observed streamflow to be relatively inaccurate (K. Shook, personal communication, 2003). Similarly, a flow hydrograph that consists of a continued low discharge level for a prolonged period probably indicates the influence of dams built by beavers at strategic locations of the upper reach of PRB. These temporary structures can alter the flow regime of a natural stream particularly during low spring snowmelt runoff.

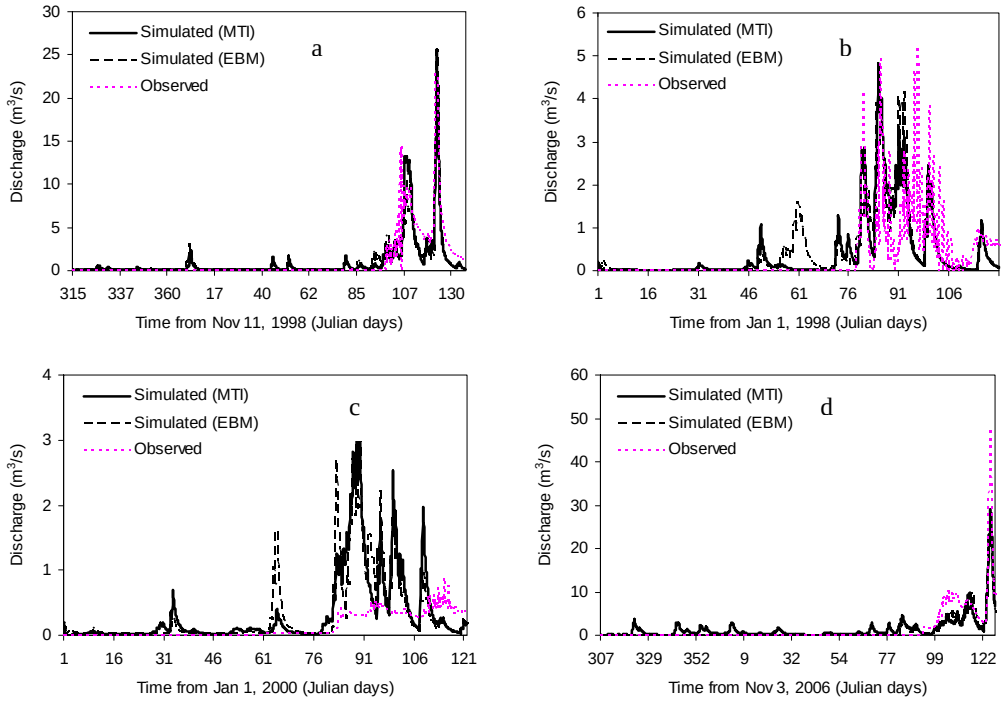

Figure 7. Comparison of observed streamflow (dotted lines) to streamflow simulated by SDSM-EBM (broken lines) and SDSM-MTI (solid lines) during model calibration (a), and validation (b to d)

The impact of incorporating T_g in the temperature index model on outflow hydrograph simulation is summarized in Table 2. When χ was set to 1 in Equation 3 (i.e. T_g is partially ignored since $T_r = T_a$) and other parameters were set at their calibrated SDSM-MTI values, R^2 dropped from 0.79 to 0.71 and E_f dropped from 0.76 to 0.71 for the calibration period of WY 1999 (see Table 2). The SDSM-MTI model in Equation 2 is reduced to the standard temperature index model (SDSM-TI) when χ is set to 1 and ψ set to 0 (i.e. T_g is completely ignored since $T_r = T_a$; M_{rf} =1). With the melt factors calibrated for SDSM-MTI, SDSM-TI achieved a R^2 and E_f of 0.3 and 0.25 respectively for WY 1999. Apparently, ψ exerts a more significant role on the influence of T_g than χ in SDSM-MTI.

Table 2. Summary statistics of the sensitivity of the temperature index models to ground temperature

Parameter	Model	R^2				*RMSE*			
		1998	1999	2000	2007	1998	1999	2000	2007
χ = 0.6, ψ = 2	MTI	0.50	0.79	0.27	0.78	3.35	1.24	4.30	1.48
χ = 1, ψ = 2	MTI[1]	0.40	0.71	0.23	0.74	2.50	1.42	3.31	1.62
χ = 1, ψ = 0	TI	0.25	0.30	0.01	0.56	4.62	2.27	4.01	2.02
χ = 1, ψ = 0	TI-R[2]	0.26	0.77	0.10	0.77	1.79	1.31	2.41	1.57

[1] The effect of ground temperature is partially ignored when χ = 1 in Equation 2.
[2] Melt factors were recalibrated for this model.

For the re-calibrated M_f based on T_a only (marked as TI-R in Table 2), SDSM-TI achieved a R^2 = 0.77, E_f =

0.75, RMSE = 1.31 for the calibration period of WY 1999. For the WY 1998 and WY 2000 validation periods, R^2 = 0.26 and 0.10, respectively. Both validation years had negative E_f. For WY 2007, the recalibrated model performed much better with R^2 = 0.77, E_f = 0.73, RMSE = 1.57. Our results confirm the contribution of T_g in modeling the basin-scale snowmelt runoff of PRB.

SUMMARY AND CONCLUSION

Three semi-distributed snowmelt models of varying degree of complexity and data requirement were developed and applied to the seasonally snow-covered, Paddle River Basin (PRB) of central Alberta. The first model is a physics-based, energy balance model (SDSM-EBM) developed to model basin scale snow accumulation and ablation processes by considering vertical energy exchange processes in open and forested areas, snowmelt processes that include liquid and ice phases separately within the snowpack, and considers canopy interception, sublimation, refreezing, snow compaction, etc. SDSM-EBM is also set up to simulate snow surface temperature. The second model is a modified temperature index approach (SDSM-MTI) that uses a reference temperature (T_r) where T_r is a weighted average of near surface soil temperature (T_g) and air temperature (T_a). The third model is the standard temperature index (SDSM-TI) method using T_a only.

In spite of their differing levels of complexity, SDSM-EBM and SDSM-MTI show strong agreement in their capability to simulate basin outflow hydrograph (Figure 7). Pearson's correlation coefficients between simulations made by the two models are 0.91, 0.96, 0.91 and 0.96 for the WY 1998, WY 1999, WY 2000 and WY 2007 winters, respectively. In view of the strong agreement between streamflows simulated by two models with very different degree of complexity, the results demonstrate that the most likely reason for the discrepancies between observed and simulated streamflow during the dry winters would be the effect of beaver dams. Field investigations conducted along the major tributaries of PRB confirmed the existence of overflow type, watertight beaver dams (Gurnell, 1998; Singh, 2002).

In terms of SWE and SD simulation, the quantitative statistics presented in Table 1 based on pooled observations for each year suggest that SDSM-MTI appears to have performed better than SDSM-EBM for most of the study years. As explained earlier, the recalibrated standard temperature index model appears to be the worst of all three models. However, only a limited number of data points used to obtain the statistics in Table 1.

In conclusion, both SDSM-MTI and SDSM-EBM are capable of simulating dependable basin-scale SWE and SD, which demonstrates the integrity of the model even though at the validation stage of WY 1998 and WY 2000 (dry winters) the simulated streamflows differ from the observed partly because of the effect of beaver dams. Apparently, compared to SDSM-MTI, the additional model complexity and relatively higher data demand of SDSM-EBM did not lead to an obvious advantage in simulating snowmelt processes for PRB. If reliable T_g data are available, it seems possible to model basin-scale snowmelt processes in the Canadian Prairies using the modified temperature index approach as accurately as the energy balance approach. However, if T_g is not available, then the energy balance approach has an advantage over the standard temperature index method, e.g., SDSM-TI that is based on air temperature (T_a) alone as the predictor for snowmelt. This is because in a Prairie environment where the snowpack depth ranges from shallow to moderate, T_g is significantly correlated to the Q_n (Singh et al., 2005) which generally dominates the energy balance for spring snowmelt in the Canadian Prairies (Shook, 1995). Furthermore, given winter in the Prairies is generally severe, T_g tends to remain at subzero level until the onset of major snowmelt during spring, which raises T_g to 0°C, as the meltwater warms up the top soil. Therefore a temperature index approach based on T_a alone cannot model the role T_g plays in the spring snowmelt process of the Canadian Prairies.

ACKNOWLEDGMENTS

This research was partly supported by equipment and operating grants from the NSERC, Canada. The first author was also partly supported by a Univ. of Alberta PhD scholarship. The third author was partly supported by the Univ. of Alberta Graduate Assistantship. Alberta Environment provided the snow pillow and streamflow data.

REFERENCES

Anderson, E.A. 1968. Development and testing of snowpack energy balance equations, Water Resources Research, 4(1), 19-37.

Bathurst, J.C., and Cooley, K.R. 1996. Use of the SHE hydrological modeling system to investigate basin response to snowmelt at Reynolds Creek, Idaho, J. Hydrol., 175, 181-211.

Beven, K.J. 1996. A discussion of distributed hydrological modeling, In: Abbott, M.B., and Refsgaard, J.C. (Eds), Distributed Hydrological Modeling, Water Resources Publications, pp. 255-278.

Biftu, G.F. and T.Y. Gan. 2001. Semi-distributed, physically-based, hydrological modeling of the Paddle River Basin, Alberta using remotely sensed data, J. Hydrol., 244, 137-156.

Blöschl, G. 1999. Scaling issues in snow hydrology, Hydrol. Process., 13, 2149-2175.

Frank, E.C. and R. Lee. 1966. Potential beam irradiation on slopes, Res. Paper RM-18, U.S. Forest Service, Washington, D.C.

Golding, D.L. and R.S. Swanson. 1986. Snow distribution patterns in clearings and adjacent forest, Wat. Resour. Res., 22, 1931-1940.

Gray, D.M. and T. Prowse. 1993. Snow and floating ice, In: Maidment D.R. (ed.), Handbook of Hydrology, McGraw-Hill Inc., New York, pp 7.1-7.58.

Gurnell, A.M. 1998. The hydrogeomorphological effects of beaver dam-building activity, Progress in Physical Geography, 22(2), 167-189.

Hardy, J.P. and K.J. Hansen-Bristow. 1990. Temporal accumulation and ablation patterns in forests representing varying stages of growth, In: Proc. of the 58th Western Snow Conference, Sacramento, CA, pp 23-34.

Hardy, J. P., R.J. Davis, R. Jordan, X. Li, C. Woodcock, W. Ni, and C. McKenszie. 1997. Snow ablation modeling at the stand scale in a boreal jack pine forest, J. Geophys. Res., 102, 29397-29405.

Hardy, J.P., R E. Davis, R. Jordan, W. Ni, and C. Woodcock. 1998. Snow ablation modeling in a mature aspen stand of the Boreal forest, Hydrol. Process., 12, 1763-1778.

Hedstrom, N. and J.W. Pomeroy. 1998. Intercepted snow in the boreal forest: measurement and modeling, Hydrol. Process., 12, 1611-1625
.
Jordan, R. 1991. A one-dimensional temperature model for a snow cover: Technical documentation for SNTHERM 89, Special Report 91-16, U.S. Army Cold Research and Engineering Laboratory, Hanover, N.H., 49 p.

Jin, J., X. Gao, S. Sorooshian, Z. Yang, R. Bales, R. Dickinson, S. Sun, and G. Wu. 1999. One-dimensional snow water and energy balance model for vegetated surfaces, Hydrol. Process. 13, 2467-2482.

Kane, D.L., R.E. Gieck, and L.D. Hinzman. 1997. Snowmelt modeling at small Alaskan arctic watershed, J. of Hydrologic Engineering, 2(4), 204-210.

Kirnbauer, R., G. Blöschl, and D. Gutknecht. 1994. Entering the era of distributed snow models, Nordic Hydrology, 25, 1-24.

Kondo J., and T. Yamazaki. 1990. A Prediction Model for Snowmelt, Snow Surface Temperature and Freezing Depth Using a Heat Balance Method, J. of Appl. Meteor., 29, 375-384.

Kustas, W.P., X. Zhan, and T.J. Schmugge. 1998. Combining optical and microwave remote sensing for mapping energy fluxes in a semiarid watershed, Remote Sens. Environ., 64, 116-131.

Martinec, J. and A. Rango. 1986. Parameter values snowmelt runoff modeling, J. Hydrol., 84, 197-219.

Pretula, B.R. and C.A. Ko. 1982. Hydrogeology of Paddle River Reservoir area near Mayerthorpe, Alberta, Alberta Environment Protection (AEP), 107 p.

Riley, J.P., E.K. Israelsen, and K.O. Eggleston. 1972. Some approaches to snowmelt prediction, AISH Publ., 2(107), 956-971.

Shook, K. 1995. Simulation of the ablation of prairie snow covers, PhD dissertation, Univ. Saskatchewan, Saskatoon, Canada, 189 p.

Singh, P.S., T.Y. Gan, and A.K. Gobena. 2005. A modified temperature index method using near-surface soil and air temperatures for modeling snowmelt in the Canadian Prairies, J. Hydrol. Engrg, 10(5), 405-419.

Singh, P.S., T.Y. Gan, and A.K. Gobena. 2009. Evaluating a hierarchy of snowmelt models at a watershed in the Canadian Prairies, J. Geophy. Res., 114, D04109, doi:10.1029/2008JD010597.

Singh, P.S. and T.Y. Gan. 2005. Modeling snowpack surface temperature in the Canadian Prairies using simplified heat flow models, Hydrol. Processes, 19, 3481– 3500.

Singh, P.S. 2002. Semi-distributed snowmelt modeling and regional snow mapping using passive microwave radiometry, PhD dissertation, Univ. Alberta, 228 p.

Tarboton D.G. and C.H. Luce. 1996. Utah Energy Balance snow accumulation and melt model (UEB), Computer model technical description and user's guide prepared by Utah Water Research Laboratory, Utah State University and USDA Forest Service, Intermountain Research Station, 64 p.

Woo, M. and J. Valverde. 1982. Ground and water temperatures of a forested mid-latitude swamp, In: Proc. of the Canadian Hydrology Symposium '82, "Hydrological Processes of Forested Areas", Fredericton, N.B., pp. 301-312.